PLUG-AND-PLAY AND RELAY REGULARIZATIONS ON NOISY LOW RANK TENSOR COMPLETION FOR SNAPSHOT MULTISPECTRAL IMAGE RESTORATION

Keisuke Ozawa

DENSO IT Laboratory

ABSTRACT

The spatial resolution of snapshot multispectral imaging is degraded owing to its spatio-spectral tradeoff. Restoring the resolution is considered as a noisy tensor completion problem and recent studies have jointly optimized the transformed tensor nuclear norm (tTNN) with regularization. However, existing work is limited and cause artifacts that stem from the periodic missing pattern and observation noise. To improve the restoration performance, we introduce two regularizations in a Plug-and-Play (PnP) manner. They still have their own drawbacks. We then further propose a Plug-and-Relay (PnR) technique to switch them at an appropriate timing. We experimentally show that PnP improves the completion accuracy compared with existing methods and that PnR could further improve the performance at a moderate computational cost.

Index Terms— Snapshot multispectral imaging, Tensor completion, Total generalized variation

1. INTRODUCTION

Snapshot multispectral imaging [1] is a key technology for spectral image analysis of dynamic scenes. However, its spatio-spectral tradeoff degrades the spatial resolution as spectral resolution increases. It is thus important to restore the spatial resolution of snapshot multispectral images [2].

Resolution restoration can be formulated as a tensor completion problem [3]. A snapshot can be converted into a three-way tensor with the full-sensor height, width, and wavelength dimension of B bands, taken from a periodic pattern with $b \times b (= B)$ filter arrays on the sensor [1]. The known entries of the tensor are sampled with the rate of $1/B$ and with just one band at a spatial position (Fig. 1 top-right). In practice, observation noise also exists. We consider snapshot data as a corrupted tensor with missing entries and Gaussian noise.

Tensor completion has been studied for image restoration and resolution enhancement. We here consider model-based approaches [4]. They generally introduce priors of global and local characterizations of data. Some types of tensor nuclear norm reflect the global low-rankness that multispectral images have. Among various models, we focus on tTNN [5, 6, 7, 8], which has attracted interest owing to its convex nature, feasibility without tuning rank-related parameters, and high performance. Since the global structure alone is not sufficient to restore a heavily corrupted tensor, recent studies [9, 3] regularized tTNN with total variation (TV) [10] to characterize the local structure and used BM3D [11] to facilitate nonlocal self-similarity [12]. They still do not consider observation noise. Only limited work on tTNN has addressed noisy tensor completion [13], where TV regularization was considered. However, it suffers from a stair-casing effect and has limited restoration ability, especially for snapshot data corrupted by its periodic missing pattern and observation noise.

In this study, we introduce two PnP [12] regularizations, total generalized variation (TGV) [14] and BM3D [15], on tTNN with considering Gaussian observation noise. TGV is a higher-order generalization of TV and improves the stair-casing effect of TV. BM3D is a state-of-the-art denoiser. They have nice properties for both completion and denoising. However, joint optimization of tTNN and these regularizations have not been investigated under noisy situation. In plugging them and analyzing the performance against snapshot data, we found that BM3D often corrupts textures in recovered images, despite its noise reduction ability. The slow computation of BM3D is another drawback. On the other hand, TGV is computed faster but is less effective for noise reduction. We overcome these drawbacks by proposing a technique of PnR regularizations, where we start with TGV in a convex fashion and then relay it to BM3D to further suppress noise. Although this technique can also be applied to the other models, we herein show the joint performance on tTNN.

We first review some backgrounds, formulate the problem, and then solve it using the alternating direction method of multipliers (ADMM) [16] when plugging TGV, BM3D, and PnR. We evaluate the performance of the regularizations on tTNN as well as against a recent completion method.

2. BACKGROUND

2.1. Definition of TNN [5, 6, 7, 8]

We denote a tensor as $\mathcal{A} \in \mathbf{R}^{n_1 \times n_2 \times n_3}$ and a matrix $\mathbf{A} \in \mathbf{R}^{n_1 \times n_2}$. For a spectral image, n_1 is the height, n_2 is the width, $n_3 = B$ is the number of bands. The k-th frontal slice is $\mathbf{A}^{(k)} = \mathcal{A}_{::k}$, and the (i, j)-th tube of $\mathcal{A}$ is a vector $\mathbf{a}^{(ij)} \in \mathbf{R}^{n_3}$. Given an invertible matrix $\mathbf{P} \in \mathbf{R}^{n_3 \times n_3}$, we have $(\mathcal{A} \times_3 \mathbf{P})_{ij:} = \mathbf{P}\mathbf{a}^{(ij)} \in \mathbf{R}^{n_3}$. Using the frontal

slice-wise matrix product $\odot_3$ and $\mathcal{T} : \mathcal{A} \mapsto \tilde{\mathcal{A}} = \mathcal{A} \times_3 \mathbf{T}$ with $\mathbf{T}$ as the matrix representation of the linear operator $\mathcal{T}$, $\mathcal{T}$-transformed tensor multiplication [5] $*_{\mathcal{T}} : \mathbb{R}^{n_1 \times n_2 \times n_3} \times \mathbb{R}^{n_2 \times m \times n_3} \to \mathbb{R}^{n_1 \times m \times n_3}$ is

$$\mathcal{A} *_{\mathcal{T}} \mathcal{B} = \mathcal{T}^{-1}(\mathcal{T}(\mathcal{A}) \odot_3 \mathcal{T}(\mathcal{B})).$$

Letting the transpose in the transformed domain be the transpose of every frontal slice, tSVD (refer the details to [5]) is

$$\tilde{\mathcal{A}} = \tilde{\mathcal{U}} \odot_3 \tilde{\mathcal{S}} \odot_3 \tilde{\mathcal{V}}^\top.$$

Then, using the matrix nuclear norm $\| \bullet \|_*$, tTNN [6] is

$$\|\mathcal{A}\|_{\mathrm{TNN}} := \frac{1}{n_3} \sum_{k=1}^{n_3} \|\tilde{\mathbf{A}}^{(k)}\|_*. \tag{1}$$

tTNN is a convex envelope [6] of the tensor average rank [17]. In this study, we use the discrete cosine transform that is used well due to its nice and balanced performance [7, 8].

2.2. Definition of TGV [14]

The second-order TGV of a tensor $\mathcal{A} \in \mathbb{R}^{n_1 \times n_2 \times n_3}$ is

$$\|\mathcal{A}\|_{\mathrm{TGV}^2_{\alpha}[\mathcal{B}]} := \alpha_0 \|\mathcal{E}(\mathcal{B})\|_1 + \alpha_1 \|\nabla \mathcal{A} - \mathcal{B}\|_1,$$
$$\mathcal{E} : \mathcal{B} \mapsto \begin{pmatrix} \partial_x \mathcal{B}_x & \frac{1}{2}(\partial_y \mathcal{B}_x + \partial_x \mathcal{B}_y) \\ \frac{1}{2}(\partial_y \mathcal{B}_x + \partial_x \mathcal{B}_y) & \partial_y \mathcal{B}_y \end{pmatrix}, \tag{2}$$

where $\mathcal{B} = (\mathcal{B}_x; \mathcal{B}_y) \in \mathbb{R}^{2n_1 \times n_2 \times n_3}$. $\nabla = (\partial_x; \partial_y)$ is the differential operator, where x and y are the spatial coordinates. It acts as $(\nabla \mathcal{A})_{ijk} = (\nabla \mathbf{A}^{(k)})_{ij}$. The L1-norms of the tensors with multiple indices for partial derivatives are $\|\mathcal{B}\|_1 = \sum_{i,j,k} \sqrt{(\mathcal{B}_x)^2_{ijk} + (\mathcal{B}_y)^2_{ijk}}$ and $\|\mathcal{E}(\mathcal{B})\|_1 = \sum_{i,j,k} \sqrt{(\mathcal{E}(\mathcal{B})_{xx})^2_{ijk} + 2(\mathcal{E}(\mathcal{B})_{xy})^2_{ijk} + (\mathcal{E}(\mathcal{B})_{yy})^2_{ijk}}$. Note that these derivatives operate along spatial dimensions. TGV regularizes first and second order derivatives, while TGV boils down to TV when $\alpha_0 = 0$ and $\mathcal{B} = \mathbf{0}$ (used for TV-TNN in Sec.5), to the second-order derivative when $\alpha_0 \to \infty$.

3. PROBLEM FORMULATION

We formulate a completion problem with the PnP [12] framework, assuming Gaussian noise to exist, as follows:

$$\mathcal{X}^* = \arg\min_{\mathcal{X}} \|\mathcal{X}\|_{\mathrm{TNN}} + \mu\varphi(\mathcal{X})$$
$$\text{s.t. } \mathcal{M} + \mathcal{N} = \mathcal{X},\ \|\mathcal{P}_\Omega(\mathcal{N})\|_F^2 < \varepsilon, \tag{3}$$

where $\mathcal{X} \in \mathbb{R}^{n_1 \times n_2 \times n_3}$ is the underlying high-resolution multispectral image and $\mathcal{M}$ is the observation. Ω is the observed entries onto which $\mathcal{N}$ is projected with $\mathcal{P}_\Omega$. $\mathcal{N}$ completes $\mathcal{M}$ and includes noise of the noise level ε, has $[\mathcal{P}_\Omega(\mathcal{N})]_{ijk} = (\mathcal{N})_{ijk}$ if $(i,j,k) \in \Omega$ and 0 otherwise. If k is the band index of the filter array, Ω has and only has the indices $\{(i, j, k(i(\mathrm{mod}\, b), j(\mathrm{mod}\, b)))|1 \le i \le n_1, 1 \le j \le n_2\}$. $\|\mathcal{A}\|_F^2 = \sum_{i,j,k} |\mathcal{A}_{ijk}|^2$ is the squared Frobenius norm of $\mathcal{A}$. φ is a regularization term weighted by some constant $\mu > 0$.

4. NOISY TENSOR COMPLETION ALGORITHM WITH PNP AND PNR REGULARIZATIONS

We solve Equation (3) following the ADMM framework [16]. From the Lagrange duality, there is a constant $\lambda > 0$ with which the augmented Lagrangian is written as

$$\mathcal{L}(\mathcal{X}, \mathcal{Y}, \mathcal{N}; \Phi_1, \Phi_2) = \|\mathcal{X}\|_{\mathrm{TNN}} + \mu\varphi(\mathcal{Y})$$
$$+ \langle \mathcal{X} - \mathcal{M} - \mathcal{N}, \Phi_1 \rangle + \frac{\rho_1}{2} \|\mathcal{X} - \mathcal{M} - \mathcal{N}\|_F^2$$
$$+ \langle \mathcal{X} - \mathcal{Y}, \Phi_2 \rangle + \frac{\rho_2}{2} \|\mathcal{X} - \mathcal{Y}\|_F^2 + \frac{\lambda}{2} \|\mathcal{P}_\Omega(\mathcal{N})\|_F^2, \tag{4}$$

where $\mathcal{Y} \in \mathbb{R}^{n_1 \times n_2 \times n_3}$ is the auxiliary variable of $\mathcal{X}$. $\Phi_i (i = 1, 2)$ are the Lagrange multipliers for constraints. $\langle \mathcal{A}, \mathcal{B} \rangle = \sum_{i,j,k} \mathcal{A}_{ijk} \mathcal{B}_{ijk}$ is the inner product between two tensors.

In solving this, we obtain the following update rules for the $(t+1)$-th iteration:

1) The update of $\mathcal{X}$ is, with $\rho'^{(t)} = \rho_1^{(t)} + \rho_2^{(t)}$,

$$\mathcal{X}^{(t+1)} = \arg\min_{\mathcal{X}} \|\mathcal{X}\|_{\mathrm{TNN}} + \frac{\rho'^{(t)}}{2} \left(\mathcal{X} - \mathcal{X}'^{(t)} \right), \tag{5}$$
$$\mathcal{X}'^{(t)} = \frac{\rho_1^{(t)}}{\rho'^{(t)}} \left(\mathcal{M}^{(t)} + \mathcal{N}^{(t)} - \frac{\Phi_1^{(t)}}{\rho_1^{(t)}} \right) + \frac{\rho_2^{(t)}}{\rho'^{(t)}} \left(\mathcal{Y}^{(t)} - \frac{\Phi_2^{(t)}}{\rho_2^{(t)}} \right)$$

This subproblem can be solved as shown in [6, 8]:

$$\mathbf{X}^{(t+1)(k)} = \mathcal{D}_{\rho'^{(t)}} \left(\mathbf{X}'^{(t)(k)} \right), \tag{6}$$

where the matrix singular value thresholding operator [18] is $\mathcal{D}_\mu(\mathbf{X}') = \mathbf{U}(\mathrm{diag}(\{\mathcal{S}'_\tau(\sigma_i)\}_{1 \le i \le r}))\mathbf{V}^\top$ against the reduced SVD as $\mathbf{X}' = \mathbf{U}(\mathrm{diag}(\{\sigma_i\})_{1 \le i \le r})\mathbf{V}^\top$. $\mathcal{S}'_\tau(x) = \mathrm{sgn}(x)(|x| - \tau)_+$ is the soft-thresholding operator [19] with $y_+ = \max(y, 0)$ operating element-wise.

2) The update of $\mathcal{N}$ is, with $\mathcal{N}'^{(t)} = \mathcal{X}^{(t)} - \mathcal{M}^{(t)} + \frac{\Phi_1^{(t)}}{\rho_1^{(t)}}$,

$$\mathcal{N}^{(t+1)} = \arg\min_{\mathcal{N}} \|\mathcal{P}_\Omega(\mathcal{N})\|_F^2 + \frac{\rho_1^{(t)}}{2} \left\| \mathcal{N} - \mathcal{N}'^{(t)} \right\|_F^2, \tag{7}$$

which is readily solved in a closed form.

3) The update of $\mathcal{Y}$ is, with $\mathcal{Y}'^{(t)} = \mathcal{X}^{(t)} + \frac{\Phi_2^{(t)}}{\rho_2^{(t)}}$,

$$\mathcal{Y}^{(t+1)} = \arg\min_{\mathcal{Y}} \frac{\mu}{\rho_2^{(t)}} \varphi(\mathcal{Y}) + \frac{1}{2} \left\| \mathcal{Y} - \mathcal{Y}'^{(t)} \right\|_F^2. \tag{8}$$

This is a PnP denoising problem. We provide solutions using TGV regularization and the BM3D denoiser; in addition, we explain how to PnR these regularizations.

Plugging TGV makes the problem convex and it can then be solved likewise using the standard ADMM [16]. Replacing the coefficients; then $(\mathcal{Y}^*, \mathcal{U}^*, \mathcal{V}^*, \mathcal{W}^*)$ should minimize

$$\frac{\rho_2^{(t)}}{2} \left\| \mathcal{Y} - \mathcal{Y}'^{(t)} \right\|_F^2 + \alpha_0 \|\mathcal{V}\|_1 + \alpha_1 \|\mathcal{W}\|_1 \tag{9}$$
$$+ \frac{\rho_3}{2} \left\| \mathcal{E}(\mathcal{U}) - \mathcal{V} + \frac{\Phi_3}{\rho_3} \right\|_F^2 + \frac{\rho_4}{2} \left\| \mathcal{W} - \nabla \mathcal{Y} + \mathcal{U} + \frac{\Phi_4}{\rho_4} \right\|_F^2,$$

where $\mathcal{U} = (\mathcal{U}_x; \mathcal{U}_y)$ is the auxiliary variable of $\nabla\mathcal{Y}$, $\mathcal{V} = (\mathcal{V}_{xx}, \mathcal{V}_{xy}; \mathcal{V}_{yx}, \mathcal{V}_{yy})$ is that of $\mathcal{E}(\mathcal{U})$, and $\mathcal{W} = (\mathcal{W}_x; \mathcal{W}_y)$ is that of $\nabla\mathcal{X} - \mathcal{U}$. The following four subproblems have closed form solutions and can be computed efficiently:

3-1) The update of $\mathcal{Y}$ is, with $\mathcal{Z}'^{(t)} := \mathcal{W}^{(t)} + \mathcal{U}^{(t)} - \frac{\Phi_4^{(t)}}{\rho_4^{(t)}}$,

$$\mathcal{Y}^{(t+1)} = \arg\min_{\mathcal{Y}} \frac{\rho_2^{(t)}}{2}\|\mathcal{Y} - \mathcal{Y}'^{(t)}\|_F^2 + \frac{\rho_4^{(t)}}{2}\|\nabla\mathcal{Y} - \mathcal{Z}'^{(t)}\|_F^2. \tag{10}$$

This subproblem can be solved in the Fourier domain.

3-2) The update of $\mathcal{U}$ includes the second order derivative:

$$\mathcal{U}^{(t+1)} = \arg\min_{\mathcal{U}} \frac{\rho_3^{(t)}}{2}\|\mathcal{E}(\mathcal{U}) - \mathcal{V}'^{(t)}\|_F^2 + \frac{\rho_4^{(t)}}{2}\|\mathcal{U} - \mathcal{U}'^{(t)}\|_F^2,$$
$$\mathcal{V}'^{(t)} := \mathcal{V}^{(t)} - \frac{\Phi_3^{(t)}}{\rho_3^{(t)}},\ \mathcal{U}'^{(t)} := \nabla\mathcal{Y}^{(t+1)} - \mathcal{W}^{(t)} + \frac{\Phi_4^{(t)}}{\rho_4^{(t)}}. \tag{11}$$

This can also be solved in the Fourier domain, but it also requires solving a simultaneous equation w.r.t. $\mathcal{U}_x$ and $\mathcal{U}_y$.

3-3) The update of $\mathcal{V}$ is, with $\mathcal{Q}^{(t+1)} = \mathcal{E}(\mathcal{U}^{(t+1)}) + \frac{\Phi_3^{(t)}}{\rho_3^{(t)}}$,

$$\mathcal{V}^{(t+1)} = \arg\min_{\mathcal{V}} \alpha_0\|\mathcal{V}\|_1 + \frac{\rho_3^{(t)}}{2}\|\mathcal{V} - \mathcal{Q}^{(t+1)}\|_F^2. \tag{12}$$

3-4) The update of $\mathcal{W}$ is a similar subproblem as (3-3), with $\mathcal{R}^{(t+1)} = \nabla\mathcal{Z}^{(t+1)} - \mathcal{U}^{(t+1)} + \frac{\Phi_4^{(t)}}{\rho_4^{(t)}}$

$$\mathcal{W}^{(t+1)} = \arg\min_{\mathcal{W}} \alpha_1\|\mathcal{W}\|_1 + \frac{\rho_4^{(t)}}{2}\|\mathcal{W} - \mathcal{R}^{(t+1)}\|_F^2. \tag{13}$$

The solutions of Equations (12) and (13) are found likewise in [20].

Plugging BM3D does not guarantee convergence naively, but allows fixed-point convergence under moderate conditions [15]; we monotonically decrease the denoising level as $\sigma^{(t)} \to 0$ $(t \to \infty)$ in iterations of applying the denoiser:

$$\mathcal{Y}^{(t+1)} = \mathcal{D}_{\sigma^{(t)}}^{\mathrm{BM3D}}(\mathcal{Y}'^{(t)}). \tag{14}$$

Plug-and-Relay addresses drawbacks of TGV and BM3D. Although BM3D is a nice implicit denoiser, we empirically found two drawbacks: first, it takes much time compared with TGV, and second, it often converges to an unexpected solution regardless of how finely the denoising level is tuned in our experiment. We consider that this is because its fixed-point convergence finds low-rank and locally self-similar patterns from the structural corruption of data. In the processes to find such patterns, we intuitively understand that the nonconvex nature and nonlinearity of plugging BM3D gradually deviate from the underlying tensor on the way from the current solutions (Fig. 1). In our PnR option, we first plug TGV until the change of variables falls below a threshold ($\mathrm{tol}_{\mathrm{switch}}$), and then start with the current solution by switching to BM3D. The first step has benefits of convexity and fast computation, and the second step has a benefit of better denoising ability.

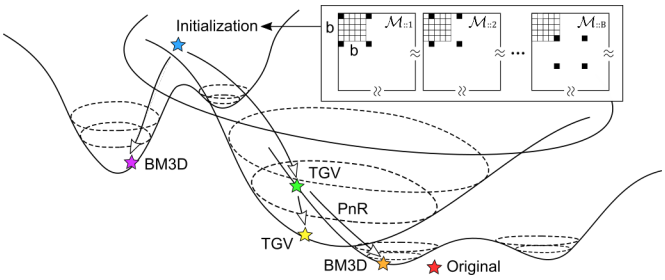

Fig. 1. Intuitive motivation to use PnR instead of PnP.

7) Finally, updates of the Lagrange multipliers are

$$\Phi_1^{(t+1)} = \Phi_1^{(t)} + \rho_1^{(t)}(\mathcal{X}^{(t+1)} - \mathcal{Y}^{(t+1)}) \tag{15}$$
$$\Phi_2^{(t+1)} = \Phi_2^{(t)} + \rho_2^{(t)}(\mathcal{X}^{(t+1)} - \mathcal{Z}^{(t+1)}) \tag{16}$$
$$\Phi_3^{(t+1)} = \Phi_3^{(t)} + \rho_3^{(t)}(\mathcal{E}(\mathbf{V})^{(t+1)} - \mathbf{U}^{(m)(t+1)})$$
$$\Phi_4^{(t+1)} = \Phi_4^{(t)} + \rho_4^{(t)}(\nabla\mathbf{Z}^{(t+1)} - \mathbf{U}^{(t+1)} - \mathcal{W}^{(t+1)}) \tag{17}$$
$$\rho_l^{(t+1)} = \min\left\{\gamma\rho_l^{(t)}, \rho_{\max}\right\} \text{ for } l = 1, 2, 3, 4, \tag{18}$$

where $\gamma > 1$ is introduced to accelerate the convergence. To sum up, we implemented Algorithm 1 with MATLAB2020b on a 64-bit, 3.20 GHz CPU desktop computer .

Algorithm 1 PnP(PnR)-TNN for noisy tensor completion

Input: Observed sparse tensor $\mathcal{M} \in \mathbb{R}^{n_1 \times n_2 \times n_3}$
Initialisation : $\mathcal{X} = \mathcal{M}$, observed tensor entries Ω;
Parameters : γ, tol, max iteration ($t_{\max}$), $\rho_{\max}$

```
while t < t_max or max change in updates > tol do
    Update X using Equation (6).
    if Plugging BM3D then
        Update Y using Equation (14).
    else if Plugging TGV then
        Update Y,U,V,W using Equations (10)-(13).
        if Plug-and-Relay and diff< tol_switch then
            Update Y using Equation (14).
        end if
    end if
    Update Z using Equation (7).
    Update the multipliers using Equations (15)-(18).
    Continue updates 2-12.
end while
```

5. EXPERIMENTS

We conducted a simulation experiment mainly for quantitative but also for qualitative comparison, and prepared real data to demonstrate the quality enhancement of recovered images.

Table 1. Comparison results on six images from CAVE dataset. **Best** and second best are emphasized.

	NL-LRTC [21]			TNTV [13]			TV-TNN			TGV-TNN			BM3D-TNN			PnR-TNN		
Scene	RSE	PSNR	SSIM	RSE	PSNR	SSIM	RSE	PSNR	SSIM	RSE	PSNR	SSIM	RSE	PSNR	SSIM	RSE	PSNR	SSIM
Flowers	0.260	25.3	0.452	0.622	19.4	0.376	0.288	25.2	0.573	0.190	28.2	**0.670**	0.205	27.6	0.657	**0.187**	**28.3**	0.667
Paints	0.214	20.4	0.509	0.216	20.1	0.629	0.238	20.3	0.651	0.158	23.0	0.753	0.164	22.4	0.771	**0.150**	**23.3**	**0.774**
Peppers	0.143	30.2	0.576	0.612	19.3	0.532	0.206	27.4	0.653	0.105	32.8	0.766	**0.084**	**34.8**	**0.844**	0.102	33.2	0.778
JellyBeans	0.338	20.9	0.523	0.531	17.0	0.391	0.327	21.2	0.606	0.230	24.1	0.730	0.284	22.6	0.681	**0.228**	**24.2**	**0.737**
Toys	0.219	21.6	0.458	0.252	20.0	0.510	0.239	21.1	0.583	0.174	23.2	0.689	0.180	23.2	0.667	**0.169**	**23.4**	**0.703**
Face	0.219	21.6	0.458	0.383	22.6	0.646	0.185	28.7	0.760	0.0763	33.5	0.840	0.0910	32.7	**0.861**	**0.0753**	**33.8**	0.850

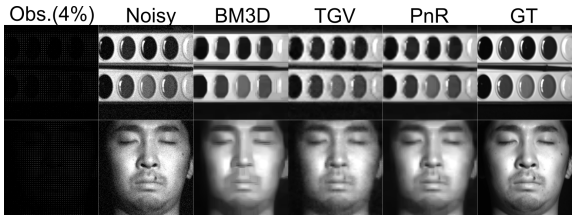

Fig. 2. Comparison of recovered images from Paints and Face.

A simulation experiment was conducted on the CAVE dataset [22]. We used representative regions of images within each 250×250 window, normalized pixel values to $[0, 1]$, added Gaussian noise with the standard deviation of 0.002, and simulated snapshots of 25 bands. We applied the proposed PnP(TGV, BM3D)-TNN and PnR-TNN, the noisy tensor completion method based on tTNN with TV (TNTV [13]), and a recent high-performance completion method using BM3D (NL-LRTC [21]). We tuned the parameters using some samples to first see the tendency roughly and then finely: for NL-LRTC, $\rho \in \{10^{-3}, 10^{-2}, 10^{-1}, 1, 10\}$ and $\sigma \in \{10, 20, 40, 80, 160\}$; for BM3D-TNN, $\lambda \in \{10, 10^2, 10^3\}$ and $\sigma^{(0)} \in \{1, 2, 4, 6, 8, 10, 12\} \times 10^4$ decaying by $1/1.1$ every iteration; and for TGV-TNN, $\alpha_0 \in \{0.1, 0.2, 0.4, 0.8, 1.6\}$ and $\alpha_1 \in \{0.1, 1\}$. The ADMM parameters were tuned within $\rho_k^{(0)} \in \{10^{-3}, 10^{-2}, 10^{-1}, 1, 10\}$ (the same over $k = 1, \cdots, 4$). Finally, for PnR-TNN, we switched to BM3D and started from $\sigma^{(0)} = 10$ with decaying by $1/1.1$. The stopping threshold was set to 10^{-4}, and among $\mathrm{tol}_{\mathrm{switch}} \in \{10^{-1}, 10^{-2}, 10^{-3}\}$, the best timing was 10^{-3}. The other parameters were the same for TGV-TNN. Since TNTV often failed using a fixed parameter considerably because it is difficult in our situation to balance the terms for low-rankness, smoothness, Gaussian, and sparse noise, we list the best values from $\rho \in \{1, 10^1, 10^2, 10^3\}$, $\gamma \in \{10^{-1}, 1, 10^1, 10^2\}$, and $\lambda \in \{1, 10^1, 10^2\}$. We also show the results from our TV-regularized implementation (TV-TNN) to clarify the effect of each regularization. We tuned within $\alpha_1 \in \{0.1, 1, 10\}$, a negligible small α_0, and $\mathcal{U} = 0$, $\rho_3^{(0)} = 1$ to balance TV, and the other parameters were the same for PnP-TNN's. We show in Table 1 the relative squared error (RSE), PSNR, and SSIM averaged over bands, against the ground truth. PnR-TNN performed the best in most cases, with TGV-TNN being the second. BM3D-TNN partly performed best against simple textures. We show two recovered images in Fig. 2. While BM3D-TNN caused artifacts, TGV-TNN recovered naturally, and PnR-TNN better reduced noise. Finally, computation took 17, 2, and 5 minutes in BM3D-, TGV-, and PnR-TNN, respectively. Our PnR technique could reduce computational cost compared with BM3D and better reduce noise than TGV.

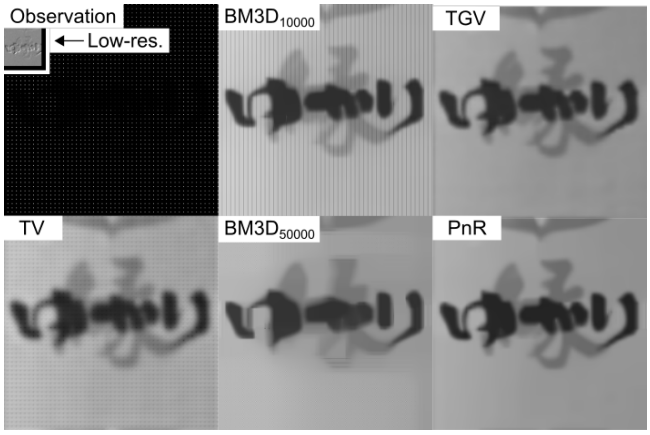

Fig. 3. Comparison between TV-, PnP(TGV, BM3D)-, and PnR-TNN with two best noise reduction levels of BM3D. In this problem, NL-LRTC [21] produced a corrupted texture (not shown).

A real experiment was conducted on snapshot data captured using a camera XIMEA MQ022HG-IM-SM5x5-NIR with 25 bands. The scene was captured similarly to the situation of [3]. A region of 250×250 pixels were recovered with our implemented TV-TNN, PnP-TNN, and PnR-TNN (Fig. 3). In all cases, spatial resolution was enhanced against the down-sampled, low resolution image. We show two best visual results of BM3D-TNN when $\sigma = 10^4$ and 5×10^4. PnR-TNN was of the best visual quality, and TGV-TNN was the second. Especially, the sharpness near edges and the contrast were enhanced in PnR compared with TGV. We consider that TGV alone could better regularize on tTNN than TV and BM3D, but PnR could further improve the performance.

6. CONCLUSION

We presented PnP- and PnR-regularized tTNN to solve a noisy tensor completion problem to restore the spatial resolution of multispectral images. Experimental results suggest that our PnP formulation improves the denoising and completion performance compared with existing methods and that the proposed PnR technique could compensate for the drawbacks of these regularizations.

7. REFERENCES

[1] L. Stefan, B. Delauré, L. Andy, and T. Nicolaas, "Hyperspectral imager development using direct deposition of interference filters," *The Small Satellites Systems and Services Symposium*, 2014.

[2] G. Tsagkatakis, M. Jayapala, B. Geelen, and P. Tsakalides, "Non-negative matrix completion for the enhancement of snapshot mosaic multispectral imagery," *electronic imaging*, vol. 2016, pp. 1–6, 2016.

[3] K. Ozawa, S. Sumiyoshi, Y. Sekikawa, K. Uto, Y. Yoshida, and M. Ambai, "Snapshot multispectral image completion via self-dictionary transformed tensor nuclear norm minimization with total variation," in *IEEE International Conference on Image Processing (ICIP)*, 2021, pp. 364–368.

[4] A. Cichocki, D. Mandic, L. De Lathauwer, G. Zhou, Q. Zhao, C. Caiafa, and H.A.PHAN, "Tensor decompositions for signal processing applications: From two-way to multiway component analysis," *IEEE Signal Processing Magazine*, vol. 32, no. 2, pp. 145–163, 2015.

[5] M. E. Kilmer, C. D. Martin, and P. Lisa, "A third-order generalization of the matrix svd as a product of third-order tensors," *Technical Report TR-2008-4, Tufts University, Department of Computer Science*, 2008.

[6] Z. Zhang, G. Ely, S. Aeron, N. Hao, and M. Kilmer, "Novel methods for multilinear data completion and de-noising based on tensor-svd," in *IEEE Conference on Computer Vision and Pattern Recognition (CVPR)*, 2014, p. 3842–3849.

[7] E. Kernfeld, M. Kilmer, and S. Aeron, "Tensor–tensor products with invertible linear transforms," *Linear Algebra and its Applications*, vol. 485, pp. 545–570, 2015.

[8] C. Lu, X. Peng, and Y. Wei, "Low-rank tensor completion with a new tensor nuclear norm induced by invertible linear transforms," in *IEEE Conference on Computer Vision and Pattern Recognition (CVPR)*, 2019, p. 5996–6004.

[9] L. Song, B. Du, L. Zhang, and L. Zhang, "A low-rank total-variation regularized tensor completion algorithm," *Communications in Computer and Information Science*, pp. 311–322, 11 2017.

[10] A. Beck and M. Teboulle, "Fast gradient-based algorithms for constrained total variation image denoising and deblurring problems," *IEEE Transactions on Image Processing (TIP)*, vol. 18, no. 11, pp. 2419–2434, 2009.

[11] X. L. Zhao, W. H. Xu, T. X. Jiang, Y. Wang, and M. K. Ng, "Deep plug-and-play prior for low-rank tensor completion," *Neurocomputing*, vol. 400, pp. 137–149, 2020.

[12] S. H. Chan, X. Wang, and O. A. Elgendy, "Plug-and-play admm for image restoration: Fixed-point convergence and applications," *IEEE Transactions on Computational Imaging*, vol. 3, no. 1, pp. 84–98, 2017.

[13] D. Qiu, M. Bai, M. K. Ng, and X. Zhang, "Robust low-rank tensor completion via transformed tensor nuclear norm with total variation regularization," *Neurocomputing*, vol. 435, pp. 197–215, 2021.

[14] K. Bredies, K. Kunisch, and T. Pock, "Total generalized variation," *SIAM Journal on Imaging Sciences*, vol. 3, no. 3, pp. 492–526, 2010.

[15] V. Katkovnik, K. Dabov, A. Foi, and K. Egiazarian, "Image denoising by sparse 3d transform-domain collaborative filtering," *IEEE Transactions on Image Processing*, vol. 16, no. 8, pp. 2080–2095, 2007.

[16] C. Wu and X. C. Tai, "Augmented lagrangian method, dual methods, and split bregman iteration for rof, vectorial tv, and high order models," *SIAM Journal on Imaging Sciences*, vol. 3, no. 3, pp. 300–339, 2010.

[17] M. E Kilmer, K. Braman, N. Hao, and R. C. Hoover, "Third-order tensors as operators on matrices: A theoretical and computational framework with applications in imaging," *SIAM Journal on Matrix Analysis and Applications*, vol. 34, no. 1, pp. 148–172, 2013.

[18] J. F. Cai, E. J. Candès, and Z. Shen, "A singular value thresholding algorithm for matrix completion," *SIAM Journal on Optimization*, vol. 20, no. 4, pp. 1956–1982, 2010.

[19] P. L. Combettes and V. R. Wajs, "Signal recovery by proximal forward–backward splitting," *SIAM Journal on Multiscale Modeling and Simulation*, vol. 4, no. 4, 2005.

[20] K. Papafitsoros, C. B. Schoenlieb, and B. Sengul, "Combined first and second order total variation inpainting using split bregman," *Image Processing On Line*, vol. 3, pp. 112–136, 2013.

[21] X. T. Li, X. L. Zhao, T. X. Jiang, Y. B. Zheng, T. Y. Ji, and T. Z. Huang, "Low-rank tensor completion via combined non-local self-similarity and low-rank regularization," *Neurocomputing*, vol. 367, pp. 1–12, 2019.

[22] F. Yasuma, T. Mitsunaga, D. Iso, and S. K. Nayar, "Generalized assorted pixel camera: Post-capture control of resolution, dynamic range and spectrum," *Technical Report, Department of Computer Science, Columbia University CUCS-061-08*, 2008.